Progress In Electromagnetics Research M, Vol. 84, 73–84, 2019

Flexible Analytical Curve-Based Dual-Band Antenna for Wireless Body Area Networks

Mohammed M. Bait-Suwailam[1, *] and Akram Alomainy[2]

Abstract—In this paper, a novel wearable inkjet printed dual-band antenna is presented, which works at 2.45 GHz and 5.8 GHz for wireless body area network applications. The proposed antenna geometry is composed of two printed monopole elements, which are constructed from an analytical profile of an exponentially-decaying sinusoidal curve. The analytically parameterized curve allows for constructing on demand irregular and unique shaped miniaturized radiators. The antenna system is printed on a transparent flexible polyethylene terephthalate (PET) film. The wearable dual-band printed antenna with an overall size $45 \times 40 \times 0.135\,\text{mm}^3$ is compact, light weight, and low profile, making it a suitable candidate for wireless body area network applications, when limited volume space for the worn unit is a requirement. Good agreement between numerical and measured data is achieved. Moreover, the overall far-field radiation performance of the wearable dual-band antenna is satisfactory, with measured peak gains of 1.81 dBi and 3.92 dBi, and total computed efficiencies of 81% and 82% at 2.45 GHz and 5.8 GHz, respectively. The effect of bending the wearable antenna structure is also investigated, and only slight performance variations are observed.

1. INTRODUCTION

One of the important keys to a reliable and successful Wireless Body-Area Networks (WBANs) implementation is the design of flexible wearable antennas, which are electrically stable when being placed on the body and are able to accommodate several frequency bands depending on application requirements [1]. Furthermore, due to the increased demands in modern wearable technology for miniature monitoring systems, antennas have to meet such needs, with a good compromise in terms of size and performance. Amongst many solutions, irregularities and uniqueness on the design and generation of antennas' prototypes need to be exploited, especially when antennas need to fit within tiny or small curved volumes. In order to meet such needs, in this work we aim to investigate the performance of an irregular dual-band antenna geometry, which is generated via analytical curve profile technique.

While majority of the wearable/non-wearable antennas proposed in the literature were based on classical radiating geometries [2–13], only a few investigated the possibility of utilizing geometrical-based analytic curves as radiators [14–21].

The work in [14] presented an inverted sinc-like geometric radiating antenna. In [15], the design of a multi-circular arc-based strips antenna was presented for multi-band operation; however, it came at the cost of narrowband impedance matching, which poses challenges when being exposed to body area networks.

Received 10 May 2019, Accepted 16 August 2019, Scheduled 24 August 2019

* Corresponding author: Mohammed M. Bait-Suwailam (msuwailem@squ.edu.om).

[1] Department of Electrical and Computer Engineering, Sultan Qaboos University, Muscat, Oman, P.O.Box 33, Al Khoud, Oman, PC 123, Oman. [2] Electrical Engineering and Computer Science Department, Queen Mary University of London, Mile End Rd, London E1 4FZ, UK.

Many other existing curve-based geometries are well known and have been extensively applied in many engineering applications, for instance meanderlines and fractal structures, as explored in [16–19], among others. In [20, 21], printed antennas based on the Chebyshev polynomials were investigated for wireless sensor nodes applications. The antennas in [20, 21] were printed on rigid substrates for single operational band. However, to the best of our knowledge, the design of a wearable dual-band antenna structure from a customized analytical curve based on an exponentially-decaying sinusoidal profile has not yet been investigated. In fact, most conventional printed antennas in literature were fabricated using printed circuit board technology on either rigid FR4 or ceramic materials, i.e., Rogers laminates. Furthermore, previous attempts of antenna designs based on planar analytic curves were studied on rigid laminates, which make them unsuitable for wearable applications. As a result, such antennas are difficult to integrate within clothing of the wearer in their present forms.

This paper demonstrates the design and performance assessment of a novel flexible and low cost inkjet printed dual-band antenna, based on customized analytic curve (see Fig. 1(a)). The antenna system is deposited on a very thin flexible Polyethylene Terephthalate (PET) film and is fed by a 50 Ω Coplanar Waveguide (CPW) structure. Numerical full-wave simulations based on CST Microwave Studio are presented and compared against measured results.

The rest of the paper is organized as follows. Section 2 presents the proposed design of the wearable dual-band antenna. Section 3 provides both numerical and experimental results, including the effect of several geometry parameters. Furthermore, the impact and performance of the wearable dual-band antenna under bending scenarios is presented. Section 4 concludes the paper with summary of the findings from this research work.

2. GEOMETRY OF THE PROPOSED ANTENNA

The proposed wearable dual-band antenna geometry is shown in Fig. 1. For modern wearable devices, inkjet printing has been one of the commercially efficient fabrication techniques for rapid fabrication of flexible antennas with high accuracy [22]. The proposed dual-band analytic-based geometry is printed on a very thin flexible PET plastic substrate. The PET thin film is made available from Mistubishi Paper Mills Ltd. (NB-WF-3GF100), and has electrical relative permittivity of 3.2 and loss tangent of $\tan\delta = 0.022$. For convenience, a finite small size substrate is chosen, which will easily fit in any wearable device, where the antenna is fed by a 50 Ω CPW structure. The designed antenna structure resides side-by-side with a finite metallic ground plane of size $L_g \times W_g$.

The antenna structure is composed of two bent planar monopole elements, spaced apart by a

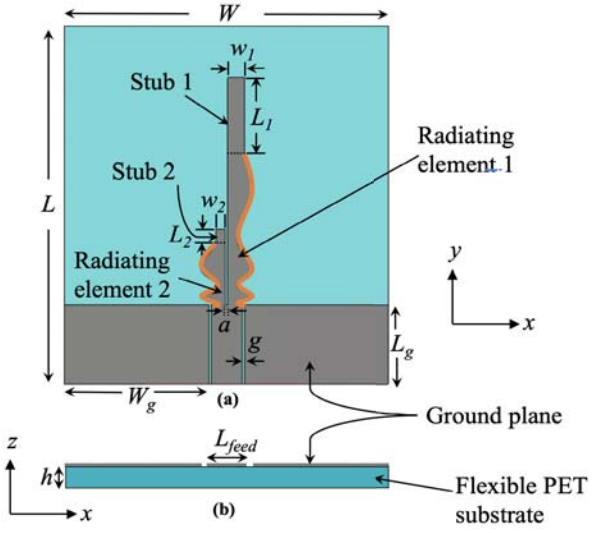

Figure 1. (a) Top view of the proposed wearable dual-band antenna along with its geometrical parameters; (b) side view of the antenna.

small finite gap, a. The two curved monopole radiating elements (see shaded curves in Fig. 1(a)) are generated from an exponentially-decaying sinusoidal profile, defined in this work by the following parametric relation:

$$\begin{aligned} x(\psi) &= \sin(2.0 * \pi * \psi), \\ y(\psi) &= \exp(\psi), \end{aligned} \tag{1}$$

where ψ is a numeric space parameter, over which the analytic curve profile of radiators is generated, and is given by:

$$\psi_{\min} \leq \psi \leq \psi_{\max}. \tag{2}$$

In this work, ψ is chosen to achieve a swept space curve to resonate close to the intended dual-band frequencies, where $\psi_{\min}$ corresponds to the starting swept point, which is fixed at 0.1 mm, while $\psi_{\max}$ corresponds to the maximum swept numeric point.

Without loss of generality and for the intended dual-band operation in this work, $\psi_{\max}$ is taken as 3 mm for the resonant analytic curved element at 2.45 GHz, and it is 2.2 mm for the resonant element at 5.8 GHz. Note that the combination of the proposed $x(\psi)$ and $y(\psi)$ analytic functions generates an exponentially-decaying sinusoidal profile, which results in a 2D planar curved layer after performing a numerical extrude process. The used sweep space range for ψ has generated two curved profiles for the dual-band antenna topology (without stubs), as shown in the right-inset of Fig. 3. The addition of the stubs has made the antenna to resonate well within 2.45/5.8 GHz WLAN bands.

Looking carefully into the curving profile in each radiating element, as shown in Fig. 1(a), the construction of the space curving profile is selectively made here in only one side per radiating element, i.e., in opposite $\pm x$ directions. In fact, the adopted analytical curve design in this proposed antenna has two advantages: firstly, the opposite profile of the curves with a small gap spacing (parameter a in Table 1) will minimize the effects of mutual coupling between the two elements and provide enhanced bandwidth. Secondly, it will maintain a reasonable omnidirectional radiation pattern for each radiating element.

Table 1. Optimized dimensions of the proposed wearable dual-band antenna.

Parameter	Unit (mm)
Substrate length, L	45
Substrate width, W	40
Substrate thickness, h	0.135
Length of ground plane, L_g	10
Width of ground plane, W_g	17.8
Length of stub 1, L_1	9.5
Width of stub 1, w_1	2.08
Length of stub 2, L_2	2
Width of stub 2, w_2	1.12
Gap between radiating elements, a	0.3
CPW feedline length, L_{feed}	3.8
CPW gap, g	0.3

For ease of tuning the antenna and for simplicity in demonstration, a small stub segment is attached to the end of each radiating element (see Fig. 1) in order to provide a tunability feature to the dual-band antenna system whenever desirable. The designed wearable dual-band antenna has been optimized in order to resonate and operate within the WLAN spectrum (2.45 GHz/5.8 GHz bands), making it a suitable candidate for WLAN/WBAN applications. Table 1 summarizes the proposed antenna geometrical parameters.

3. NUMERICAL AND EXPERIMENTAL RESULTS

3.1. Antenna Prototype

Figure 2(a) shows an image of the fabricated dual-band antenna prototype, where an edge-fed SMA connector is used for feeding the fabricated antenna using conductive expoxy paste. The antenna is fabricated using an inkjet Dimatix material printer, which is considered one of the low cost, recycleable, and precise prototyping tools for flexible antennas fabrication. A closer look into the deposited silver nanoparticles can be seen in Fig. 2(b), in which reasonable smooth conductive silver-based layer is maintained. In practice, the conductivity of the deposited silver nanoparticles may vary from $0.4 \sim 2.5 \times 10^7$ S/m, depending on temperature, duration of sintering, and number of printed silver layers [22, 23]. Note that two repeated conductive silver layers are considered in the fabrication process in order to maintain good electrical conductivity for the metallic silver particles, after which heat sintering using an iron pressing is applied to produce sufficient conductivity of metallic silver layer.

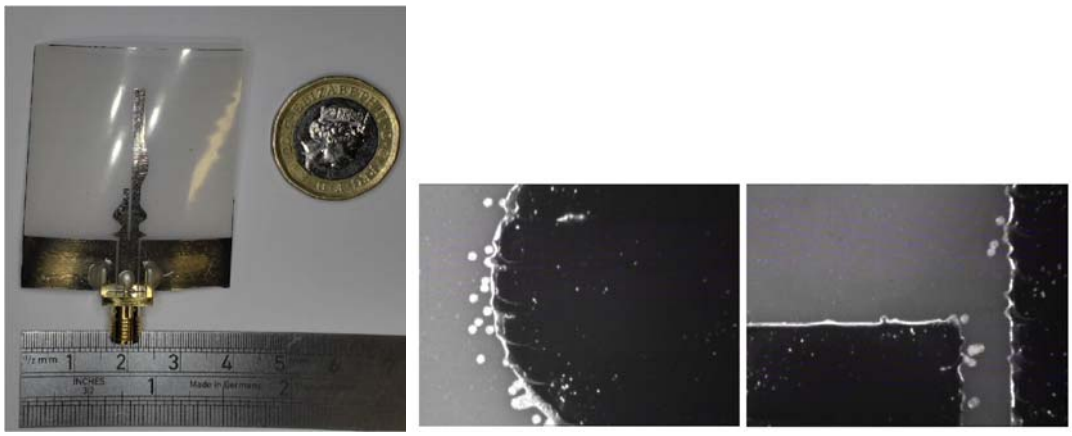

(a) (b)

Figure 2. (a) An image of the fabricated wearable dual-band antenna; (b) A microscopic close-up image showing the deposited silver nanoparticles layer.

Within the numerical full-wave simulations, the antenna is excited through a 50 Ω coplanar wave port. Furthermore, the material of the metallic radiators is assigned as silver in order to mimic the fabricated antenna prototype, where conductive silver nanoparticles are deposited in the flexible PET substrate.

3.2. Scattering Parameters Results

Figure 3 shows the numerically computed reflection coefficient of the dual-band antenna validated with measured results. Good agreement between the simulated and measured data is achieved. From Fig. 3, the proposed antenna yields measured impedance bandwidth of 34% (1.86–2.63 GHz) covering the first resonance and achieves a wide impedance bandwidth of 44% covering the second resonance (5.09–8.0 GHz). The case of the dual-band antenna without stubs is also numerically evaluated, as shown in Fig. 3, in which it operates off the 2.45 and 5.8 GHz WLAN bands.

Snapshots of the electric surface current distribution for the proposed flexible antenna at its dual-frequency bands are also presented in Fig. 4. As can be seen from Figs. 4(a), (b), significant surface current distribution is observed, within both radiating curved monopole elements, with minimal coupling effects.

Next, the performance of the proposed dual-band analytical-based antenna in terms of its impedance bandwidth is compared against that of a conventional (i.e., flat) dual-monopole antenna structure, as shown in Fig. 5(b). For an adequate comparison, the flat dual-monopole antenna radiating

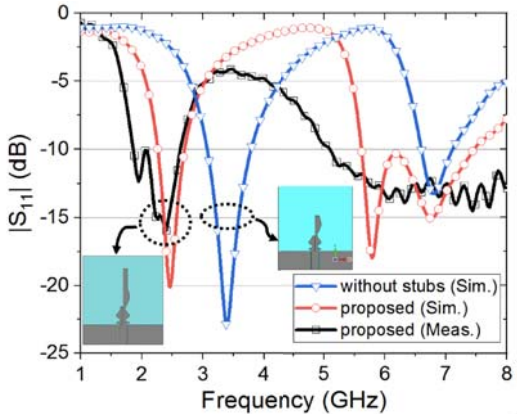

Figure 3. Simulated versus measured reflection coefficient of the proposed wearable dual-band antenna, and compared against the antenna case without stubs.

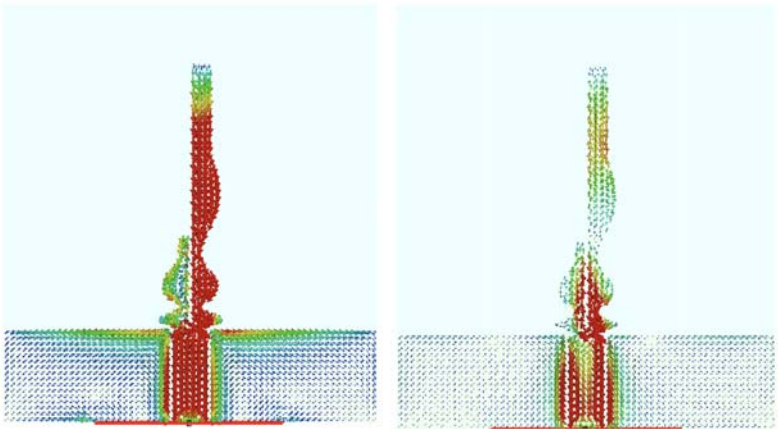

Figure 4. Snapshot of computed surface current distribution for the wearable dual-band antenna at phase 0° at: (a) first resonance, 2.45 GHz, and (b) second resonance, 5.8 GHz.

structure is printed on a similar flexible substrate with same dielectric properties and dimensions as the proposed antenna host material including ground metallization layer and feeding structure. Fig. 5(a) shows the simulated reflection coefficient, $|S_{11}|$, of the proposed antenna and the conventional (flat) dual-band resonant monopole antenna. As can be seen from Fig. 5(a), the proposed antenna has an operational impedance bandwidth of 19.3% at 2.45 GHz, while the conventional antenna has its first resonance dip at 2.61 GHz and hence out of the band of 2.45 GHz frequency band. Moreover, the proposed antenna's impedance bandwidth at frequency of 5.8 GHz is 32.3%, while it is narrowband with only 5.8% for the conventional dual-band monopole antenna structure. We also note here that the resonance dip at 5.8 GHz is almost the same for both antennas. Based on this numerical full-wave study, the proposed antenna provides wider bandwidth at both operational frequency regimes than the conventional dual-band antenna. We also note that due to the wideband impedance matching of the proposed flexible analytical-based antenna covering its second resonance band (5.8 GHz), it can be adopted for ultra-wideband applications.

3.3. Variation of Antenna Geometrical Parameters

In this part, numerical parametric analysis focusing on the effects of length of stubs L_1 and L_2 on the dual-band antenna resonances is conducted and presented in Table 2. As expected, reducing the stub length, L_1 results in shifting the first resonance at 2.45 GHz towards higher frequencies. For

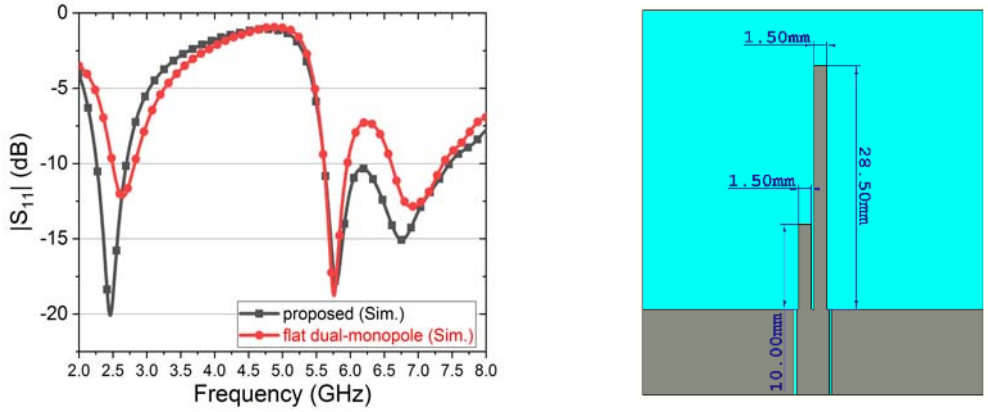

(a) (b)

Figure 5. (a) Simulated reflection coefficient of the proposed wearable dual-band antenna and compared against a conventional dual-monopole antenna; (b) top view of the conventional flat dual-monopole antenna with its dimensions. Note that gray area represents silver metallization layer.

Table 2. Numerical parametric studies for the effect of stub lengs on the proposed antenna dual-resonances.

Parameters (in mm)	Resonance dip (GHz)	% in resonance shift w.r.to f_o
Stub length L_1 =		$f_o = 2.45$ GHz
9.5	2.47	0.82
7.5	2.63	7.35
5.5	2.79	13.8
3.5	2.98	21.63
Stub length L_2 =		$f_o = 5.8$ GHz
2.0	5.8	-
1.5	6.03	3.96
1.0	6.28	8.28
0.5	6.59	13.62

instance, with a stub length of $L_1 = 3.5$ mm, the dip of the first resonance is noted at 2.98 GHz. Similar observations are also observed for the case of varying the stub length, L_2, representing the second resonance frequency at 5.8 GHz. For the case of $L_2 = 2.0$ mm, resonance dip of -19.25 dB is located at 5.8 GHz.

It is worth noting here that the addition of the two end stubs, L_1 and L_2 provides an extra freedom to the proposed antenna, in such a way that changing the stub length of any curved radiating element does not affect the other resonant frequency. Moreover, due to the nature of the curvature profile of the proposed analytical-based radiating elements, this has added extra design flexibility in the width of the radiating elements as compared to the conventional dual-monopole antenna geometry (see Fig. 5(b)), where the latter is constrained by the compact edges of the center conducting feedline of the CPW structure.

3.4. Bending Effects

It is essential that wearable antennas maintain good performance when being attached to particular surfaces or in bending conditions. In this section, the effect of bending the wearable dual-band antenna on top of a Styrofoam layer as well as a cylinder-shaped PVC has been experimentally investigated.

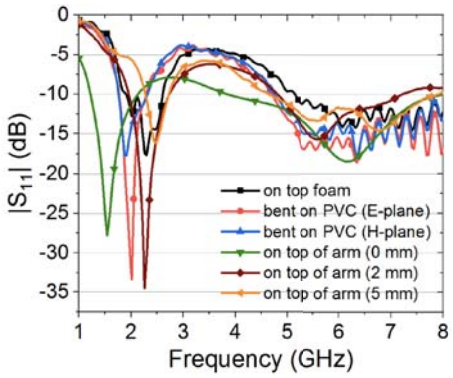

Figure 6. Measured reflection coefficient showing the effects of bending the proposed antenna on top of foam, PVC (E-plane), PVC (H-plane), and when in close-proximity to human arm.

Figure 7. An image of the proposed flexible antenna on top of a subject arm for illustration purposes.

Fig. 6 shows measured results for the reflection coefficient of the antenna when being bent on top of a semi-cylindrical styrofoam with flat base (radius = 10 mm) as well as on top of PVC cylinder (radius = 37.5 mm and height = 26 mm) in both E- and H-planes. As can be seen from Fig. 6, antenna's dual-band resonances are unaltered in the case of bending against foam layer as expected. Only a slight shift in antenna's first resonance dip is observed for the case of PVC bending, where stronger resonance behavior is observed for the E-plane bending case than the resonance dip in the H-plane bending scenario. However, this can be resolved by slightly reducing the stub length, L_1. Note that the E-plane bending corresponds here to bending the antenna along the longitudinal side (i.e., along the PVC height), while H-plane bending corresponds to the perpendicular antenna bending orientation to longitudinal direction.

Moreover, the performance of the antenna when placed on top of a human arm has also been assessed by measuring the reflection coefficient when the wearable antenna is in contact with arm and on top of the arm by 2 mm and 5 mm, as shown in Fig. 6. For illustration purposes, an image of the antenna on top of the subject arm of a male volunteer is shown in Fig. 7, where very thin transparent tape is used in order to maintain stability of the antenna on top of the subjected arm. Based on the experimental results in Fig. 6, the antenna shows satisfactory performance, except that the resonance dip at 2.45 GHz is noticed to shift to lower frequencies for the case of the antenna on top of the arm, i.e., direct contact with the arm. This is attributed to the very small thickness of the PET film when in contact with very lossy human tissues.

3.5. Far-Field Radiation Properties

The far-field properties of the proposed dual-band antenna are presented and discussed next. Fig. 8 depicts computed 2D polar radiation patterns of the wearable antenna in two principal cut planes, E- and H-planes, at 2.45 GHz and 5.8 GHz. As shown from the normalized radiation patterns in Fig. 8, the antenna has a monopole-like pattern, with a consistent omnidirectional coverage in both E- and H-planes. The measured radiation patterns of the antenna agree quite well with the simulated ones. Moreover, several ripples are observed in the measured H-plane patterns at 2.45 GHz. This is attributed to the unpredicted conductivity of silver nanoparticles as well as the inherent dielectric properties of the adopted PET laminate.

The peak gain and total efficiency of the antenna at 2.45 GHz and 5.8 GHz are also computed, where gains of 2.05 dBi and 3.63 dBi, and efficiencies of 81% and 82% are obtained at 2.45 GHz and 5.8 GHz, respectively. For validation purposes, the peak gain of the proposed antenna is measured using gain transfer method, which is 1.81 dBi and 3.92 dBi at 2.45 GHz and 5.8 GHz, respectively, agreeing well with the calculated ones. For comparison purposes, the peak gain of the conventional dual-monopole antenna (as shown in Fig. 5(b)) at its dual-operational frequencies is numerically calculated. The peak

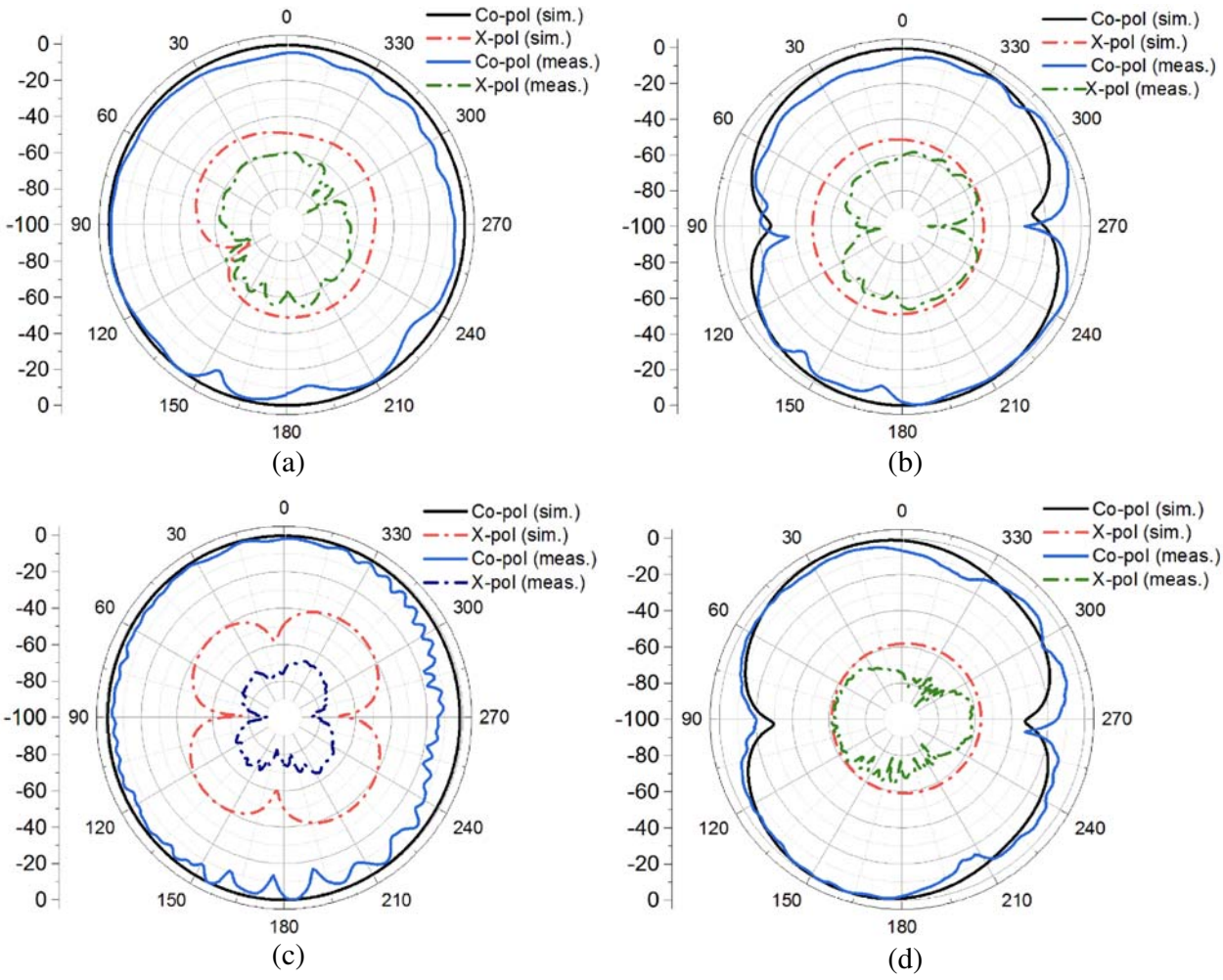

Figure 8. Measured and simulated radiation patterns for the proposed wearable dual-band antenna: at 2.45 GHz (a) E-plane (xoz), (b) H-plane (yoz); and at 5.8 GHz (c) E-plane (xoz), (d) H-plane (yoz).

gain at its first resonance is 2.0 dBi, while it is 3.2 dBi at the second resonance frequency, which is lower than the peak gain of the proposed analytical-based antenna by almost 0.5 dBi at the same resonance frequency of 5.8 GHz.

3.6. SAR Calculation

In order to investigate the performance of the proposed wearable dual-band antenna when on-body contact, Specific Absorption Rate (SAR) is numerically studied. SAR quantifies the amount of electromagnetic power that is absorbed by human tissues, and it is averaged either over the whole body or over a small tissue volume (typically 1-gram or 10-gram tissue mass). SAR can be numerically calculated from the electric field within the tissue:

$$\mathrm{SAR} = \sigma.|E|^2/\rho, \tag{3}$$

where σ is the electrical conductivity of sample tissue (in S/m), E the RMS electric field (in V/m), and ρ the density of tissue (in kg/m^3). In this study, numerical simulations for a 10-g averaged peak SAR at different accepted input power levels are carried out.

Figure 9 depicts a simplified numerical setup to study the maximum absorption rate from the flexible antenna in close proximity to multilayer human subject tissues. Within the numerical setup, the antenna is placed on top of a modeled human arm, consisting of three layers: skin (2 mm thick), fat

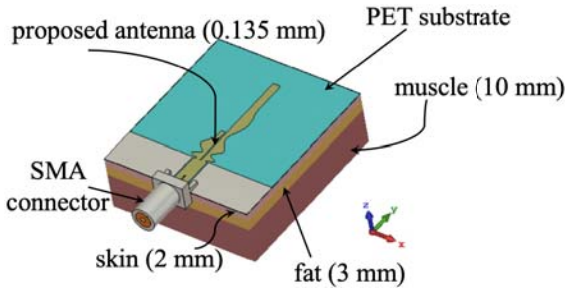

Figure 9. Numerical setup model to study SAR for the flexible antenna on top of a modeled multilayer arm, comprising skin, fat and muscle tissues.

(3 mm thick), and muscle (10 mm thick), in which all electrical properties of those tissues are obtained from the Institute of Applied Physics datasheet [24]. Further, the antenna is made in contact with the modeled arm with no spacing or shielding materials. For convenience and numerical computational resources, the size of the modeled arm is considered as $40 \times 45 \times 22\,\text{mm}^3$ (in x, y and z, respectively). The obtained peak SAR values are presented in Table 3 for various accepted input power levels.

Table 3. Peak SAR results for the dual-band antenna on top of a modeled human arm under different accepted power levels.

Incident Power (mW)	10-g averaged SAR (W/kg)	
	2.45 GHz	5.8 GHz
10	0.620	0.700
25	1.551	1.750
50	3.101	3.499
100	6.203	6.998

As expected, the obtained SAR levels show that the amount of electromagnetic energy absorbed by the tissues increases, as the input power increases. Based on the numerical results, the obtained maximum absorption rate values (in W/kg) at 2.45 GHz are 0.620, 1.551, 3.101, and 6.203, for the incident power levels of 10, 25, 50, and 100 mW, respectively. We highlight here that the 10-g averaged SAR levels are below 4 W/kg. According to ICNIRP safety levels for maximum SAR averaged over 10-g of tissue for hands, feet, and wrists [25], the obtained peak SAR levels are within acceptable safety limits for the input power levels of less than 100 mW. High peak SAR levels are observed from the antenna when input power level reaches 100 mW. Nevertheless, SAR levels will gradually decrease as we increase the spacing between the antenna and human tissue, in which a very thin foam spacer can be used to provide further stability to the antenna. In other words, input power can easily be increased, if an extra spacing is added between the antenna and the tissue. For comparison purpose and for worst case scenario, the peak SAR values for the conventional flat dual-band monopole antenna are calculated as 6.035 W/kg and 7.173 W/kg at 2.45 GHz and 5.8 GHz, respectively, under accepted input power level of 100 mW. Such computed figures are comparable to the peak SAR levels obtained using the proposed analytical dual-band antenna as presented in Table 3.

For illustration purposes, three-dimensional maximum absorption rate distributions from the proposed antenna at the antenna's dual resonance frequencies (under an accepted power level of 25 mW) are displayed in Fig. 10. As can be seen from Figs. 10(a), (b), most of electromagnetic field penetration into the tissues is observed in the volume nearest to the end of the ground plane. The far-field performance of the antenna on top of the modeled arm without any spacing is deteriorated. This is due to several factors. Firstly, human tissues are in principle very lossy with very high dielectric profile,

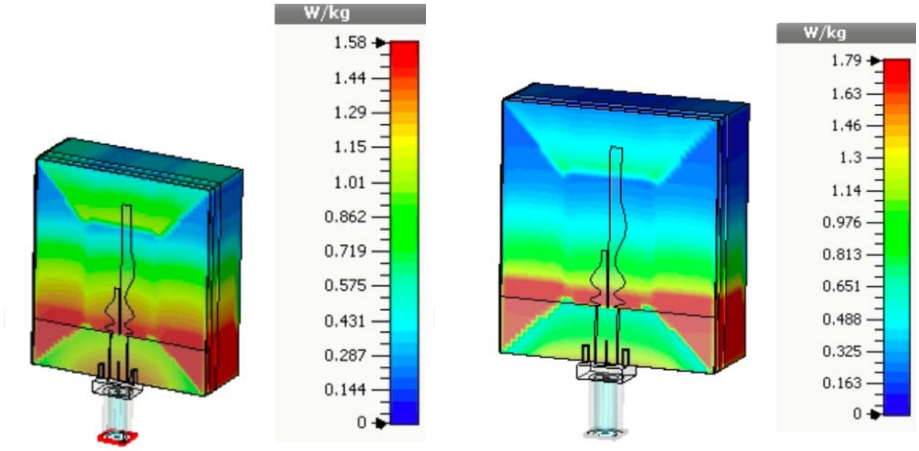

Figure 10. 3D SAR patterns at the antenna's dual resonance frequencies: (a) 2.45 GHz, and (b) 5.8 GHz, at incident power level of 25 mW. The 2D maximum SAR levels can be seen in the insets.

Table 4. Comparison of proposed antenna with other selected published works.

Reference	Proposed structure	Operating freqs. (GHz)	Antenna dimension (mm^3)	Fabrication	Max. Gain (dBi)
[2]	PIFA	2.45	$40 \times 30 \times 0.236$	sleeve cloth	2.1
[3]	regular patch	2.4	$76 \times 71 \times 3$	knitted-copper fabric	N/A
[5]	patch on top of EBG	2.45/5.8	$55 \times 55 \times 3.3$	Zelt-sewen fabric	6.4/7.6
[9]	conductive patch	2.45	$50 \times 50 \times 3.94$	flexible foam substrate	6.06
[10]	dual-monopoles	2.45/5.8	$20 \times 32.5 \times 0.156$	inkjet	N/A
[11]	ring Z-shaped	0.9/2.4	$87 \times 54 \times 0.05$	inkjet	16.24
[12]	polygon-patch	0.9/1.8	$240 \times 240 \times 1$	conductive tape on jeans fabric	N/A
[13]	patch with multi-rings	2.5/4.5	$15 \times 14 \times 0.17$	ink-based printing	$-5.34/-4.49$
[19]	curved meanderline	0.47/1.33	$110 \times 90 \times 0.088$	conductive-thread sewn on fabric	N/A
[20]	smooth sinusoidal monopole	2.5	$30 \times 20 \times 1.6$	rigid FR4 (PCB)	2.6
Proposed	**exponentially sinusoidal profile**	**2.45/5.8**	$45 \times 40 \times 0.135$	**inkjet**	**1.81/3.92**

which are unavoidable. Secondly, the antenna design does not require any ground plane reflector, which is a design requirement for ease of integration with flexible electronics along with the adopted PET thin film of 0.135 mm-thickness.

From this SAR analysis, we note here that the proposed antenna is well suited for low-power applications, such as wearable health care devices. In Table 4, a comparison summary of the proposed antenna with several selected published works is provided. It can be seen that the proposed antenna provides low-cost solution of a very thin and flexible prototype based on analytical customized curved profile with acceptable performance compared to other presented antennas in literature.

4. CONCLUSION

In this paper, a novel flexible wearable inkjet printed dual-band antenna is presented, operating at 2.4 GHz and 5.8 GHz WLAN applications. The designed antenna is composed of two printed monopole elements based on a customized analytical geometric curve, which is generated using an exponentially-decaying sinusoidal profile.

Good agreement between numerical full-wave simulations and measured results is achieved. Based on the achieved results, the proposed antenna provides good performance with wide impedance bandwidth, even in bending conditions. The measured peak gains of the antenna are 1.81 dBi and 3.92 dBi at 2.45 GHz and 5.8 GHz, respectively. Moreover, 10-g averaged SAR of a modeled human arm is numerically considered and calculated at different input power levels and within the standard safety limits for input power levels below 100 mW, when the antenna is in direct contact with body tissue.

ACKNOWLEDGMENT

The first author acknowledges the support of Sultan Qaboos University, Oman in granting him research leave to accomplish this research work.

REFERENCES

1. Hall, P. S. and Y. Hao, "Antennas and propagation for body centric communications," *2006 First European Conference on Antennas and Propagation*, 1–7, Nov. 2006.
2. Salonen, P. and J. Rantanen, "A dual-band and wide-band antenna on exible substrate for smart clothing," *Conference of the IEEE Industrial Electronics Society (IECON)*, Vol. 1, 125–130, Feb. 2001.
3. Salonen, P. and A. Hume, "A novel fabric WLAN antenna for wearable applications," *2003 IEEE Antennas and Propagation Society Symposium*, 700–703, 2003.
4. De Cos, M. E. and F. Las-Heras, "Polypropylene-based dual-band CPW-Fed monopole antenna [Antenna Applications Corner]," *IEEE Antennas and Propagation Magazine*, Vol. 55, No. 3, 264–273, Jun. 2013.
5. Zhu, S. and R. Langley, "Dual-band wearable textile antenna on an EBG substrate," *IEEE Trans. Antennas Propag.*, Vol. 57, 926–935, 2009.
6. Chauraya, A., W. G. Whittow, J. Vardaxoglou, Y. Li, R. Torah, K. Yang, S. Beeby, and J. Tudor, "Inkjet printed dipole antennas on textiles for wearable communications," *IET Microwaves, Antennas and Propagation*, Vol. 7, No. 9, 760–767, 2013.
7. Rida, R. V. M. A., L. Yang, and M. Tenzeries, "Conductive inkjet-printed antennas on low-cost paper-based substrates for RFID and wsn applications," *IEEE Antennas and Propagation Magazine*, Vol. 51, No. 3, 13–23, 2009.
8. Hettak, K., T. Ross, R. James, A. Momciu, and J. Wight, "Flexible polyethylene terephthalate-based inkjet printed CPW-fed monopole antenna for 60 GHz ISM applications," *2013 European Microwave Integrated Circuit Conference*, 476–479, Oct. 2013.
9. Hertleer, L. V. C., H. Rogier, and L. V. Langenhove, "A textile antenna for off-body communication integrated into protective clothing for fire-fighters," *IEEE Trans. Antennas Propag.*, Vol. 57, 919–925, 2009.
10. Rida, A., G. Shaker, F. Nasri, T. Reynolds, S. Nikolaou, and M. Tenzeris, "Inkjet printing of dual band conformal antenna for use in WiFi frequency bands," *2010 IEEE Radio and Wireless Symposium (RWS)*, 65–67, Jan. 2010.
11. Hassan, A., S. Ali, G. Hassan, J. Bae, and C. Lee, "Inkjet-printed antenna on thin PET substrate for dual band Wi-Fi communications," *Microsystem Technologies*, Vol. 23, No. 8, 3701–3709, Aug. 2016.
12. Sundarsingh, E., S. Velan, M. Kanagasabai, A. Sarma, C. Raviteja, and M. Alsath, "Polygon-shaped slotted dual-band antenna for wearable applications," *IEEE Antennas and Wireless Prop. Letters*, Vol. 13, 611–614, 2014.

13. Haerinia, M. and S. Noghanian, "A printed wearable dual-band antenna for wireless power transfer," *Sensors*, Vol. 19, 1732:10, 2019.
14. Badhai, R. K. and N. Gupta, "Design of wideband inverted Sinc shaped monopole antenna," *2014 Fourth International Conference on Communication Systems and Network Technologies*, 34–37, Apr. 2014.
15. Verma, S. and P. Kumar, "Compact arc-shaped antenna with binomial curved conductor-backed plane for multiband wireless applications," *IET Microwaves, Antennas Propagation*, Vol. 9, No. 4, 351–359, 2015.
16. Gianvittorio, J. P. and Y. Rahmat-Samii, "Fractal antennas: A novel antenna miniaturization technique, and applications," *IEEE Antennas and Propagation Magazine*, Vol. 44, No. 1, 20–36, Feb. 2002.
17. Jerzy Guterman, A. A. M. and C. Peixeiro, "Microstrip fractal antennas for multistandard terminals," *IEEE Antennas and Wireless Propagation Letters*, Vol. 3, 351–354, 2004.
18. Chien, H., C. Sim, and C. Lee, "Dual-band meander monopole antenna for WLAN operation in laptop computer," *IEEE Antennas and Wireless Propagation Letters*, Vol. 12, 694–697, 2013.
19. Georget, E., R. Abdeddaim, and P. Sabouroux, "Analytical, simulation and measurement studies of a dual-band open-sleeve curved meander line antenna on a exible substrate," *Progress In Electromagnetics Research*, Vol. 145, 49–57, 2014.
20. Kakoyiannis, C. G. and P. Constantinou, "Radiation poperties and ground-dependent response of compact printed sinusoidal antennas and arrays," *IET Microwaves, Antennas and Propagation*, Vol. 4, No. 5, 629–642, May 2010.
21. Kakoyiannis, C. G. and P. Constantinou, "Compact WSN antennas of analytic geometry based on Chebyshev polynomials," *2012. Loughborough Antennas Propagation Conference (LAPC)*, 1–6, Nov. 2012.
22. Yang, L., A. Rida, R. Vyas, and M. M. Tentzeris, "RFID tag and RF structures on a paper substrate using Inkjet-printing technology," *IEEE Transactions on Microwave Theory and Techniques*, Vol. 55, No. 12, 2894–2901, Dec. 2007.
23. Shaker, G., S. Safavi-Naeini, N. Sangary, and M. M. Tentzeris, "Inkjet printing of ultrawideband (UWB) antennas on paper-based substrates," *IEEE Antennas and Wireless Propagation Letters*, Vol. 10, 111–114, 2011.
24. Institute of Applied Physics. (accessed on 20 June, 2019), [Online], Available: http://niremf.ifac.cnr.it/tissprop/htmlclie/htmlclie.
25. Institute of Electrical and Electronics Engineers (IEEE), IEEE Standard for Safety Levels with Respect to Human Exposure to Radio Frequency Electromagnetic Fields, 3 kHz to 300 GHz (IEEE Std C95.1-2005), IEEE: Piscataway, NJ, USA, 2006.